LAWRENCE
LIVERMORE
NATIONAL
LABORATORY

LLNL-JRNL-701340

Comparisons between tokamak fueling of gas puffing and supersonic molecular beam injection in 2D simulations

Y. L. Zhou, Z. H. Wang, X. Q. Xu

August 24, 2016

Physics of Plasmas

Disclaimer

This document was prepared as an account of work sponsored by an agency of the United States government. Neither the United States government nor Lawrence Livermore National Security, LLC, nor any of their employees makes any warranty, expressed or implied, or assumes any legal liability or responsibility for the accuracy, completeness, or usefulness of any information, apparatus, product, or process disclosed, or represents that its use would not infringe privately owned rights. Reference herein to any specific commercial product, process, or service by trade name, trademark, manufacturer, or otherwise does not necessarily constitute or imply its endorsement, recommendation, or favoring by the United States government or Lawrence Livermore National Security, LLC. The views and opinions of authors expressed herein do not necessarily state or reflect those of the United States government or Lawrence Livermore National Security, LLC, and shall not be used for advertising or product endorsement purposes.

LLNL-JRNL-701340

Comparisons between tokamak fueling of gas puffing and supersonic molecular beam injection in 2D simulations

Y L Zhou[1,2], Z H Wang[2], X Q Xu[3],H D Li[4], H Feng[4],W G Sun[1,4]

[1]*Institute of Atomic and Molecular Physics, Sichuan University, Chengdu 610041, China*

[2]*Southwestern Institute of Physics, Chengdu 610041, China*

[3]*Lawrence Livermore National Laboratory, Livermore, CA 94550, USA*

[4]*School of Physics and Chemistry, Xihua University, Chengdu 610041, China*

Email: zhouyulinhj@sina.cn; zhwang@swip.ac.cn

Abstract

Plasma fueling with high efficiency and deep injection is very important to enable fusion power performance requirements. It is a powerful and efficient way to study neutral transport dynamics and find methods of improving the fueling performance by doing large scale simulations. Two basic fueling methods, gas puffing (GP) and supersonic molecular beam injection (SMBI), are simulated and compared in realistic divertor geometry of the HL-2A tokamak with a newly developed module, named *trans-neut*, within the framework of BOUT++ boundary plasma turbulence code [Z. H. Wang et al., Nucl. Fusion 54(2014) 043019]. The physical model includes plasma density, heat and momentum transport equations along with neutral density and momentum transport equations. Transport dynamics and profile evolutions of both plasma and neutrals are simulated and compared between GP and SMBI in both poloidal and radial directions, which are quite different from one and the other. It finds that the neutrals can penetrate about four centimeters inside the last closed (magnetic) flux surface (LCFS) during SMBI, while they are all deposited outside of the LCF during GP. It is the radial convection and larger inflowing flux which lead to the deeper penetration depth of SMBI and higher fueling efficiency compared to GP.

Keywords: plasma fueling, GP and SMBI simulations, neutral transport, injection depth, convection velocity

1. Introduction

To enable fusion power performance requirements for next generation devices, like ITER, plasma fueling with higher efficiency and deeper penetration is crucial. There are usually three main fueling methods such as pellet injection (PI) [1], gas puffing (GP) [2] and supersonic molecular beam injection (SMBI) [3]. The condensed hydrogen pellets can deeply penetrate into the core plasma with a high injection velocity. But it's more expensive and needs more complex equipment than the other two methods. GP does not require many complex techniques and does not cost so much, but it's hard to get a deep injection and a high injecting efficiency. As a new fueling method, SMBI has been developed firstly in the HL-1M tokamak and then used broadly in other tokamaks such as ASDEX Upgrade [4, 5] and JT-60U [6, 7]. It has been proved that SMBI increases the penetration depth (i.e., 500-1200ms^{-1}) and fueling efficiency with a larger injection speed compared to GP. According to fueling particle inventory [8] of experiment, a larger percentage of fueling particles can be injected deeper into the plasma by SMBI. The fueling efficiency of SMBI can be up to $30-60\%$. It is also found recently that SMBI is a good tool for edge localized mode (ELM) control and mitigation [9].

As it is said above, comparison of these fueling methods can be made in experiments. A fast TV camera and a charge exchange recombination spectroscopy (CXRS) [6, 7] are used to detect the penetration of fueling particles in the experiment. However, there are many important physical processes, the penetration front of neutrals, 2D/3D transport dynamics of particles and their collisional interactions, which cannot be directly measured in the experiment due to technical problems and complicated plasma environment. There have been several codes to study neutral transport and interactions with plasma during GP such as B2 [10], UEDGE [11,12] and TOKES[13] etc. There are a few modeling program and codes being able to simulate SMBI, except the BOUT++ code which has recently developed one new module, named *trans-neut* [15], to study the 3D transport dynamics during SMBI in real tokamak geometry. It modifies the BOUT++ code of boundary plasma turbulence (i.e., ELMs [14]) on microscopic scales to study also the transport dynamics on macroscopic scales. The basic reactions among hydrogen molecules, atoms and plasma are included in the simulations. The basic boundary conditions are also considered, such as constant flux boundary condition, particle recycling boundary conditions and sheath boundary conditions.

It is critical to understand neutral transport dynamics and find methods of improving the fueling performances especially for high efficiency and deep injection. In this paper, GP and SMBI have been simulated and compared in realistic divertor geometry of the HL-2A tokamak with the *trans-neut* module of BOUT++ code. Plasma initial states are the same for both GP and SMBI. For constant flux injection boundary conditions, SMBI has a much larger radial injection speed and a larger injecting molecular flux than GP. The physical model of transport equations and the boundary conditions are described in section 2. Simulation results of transport dynamics and profile evolutions during GP and SMBI will be compared in

section 3. Finally, results are summarized in section 4.

2. Physical model

2.1 Transport equations

During fueling, the collisional reactions among plasmas, atoms and molecules are very complicated. It is difficult to simulate the transport dynamics of fueling with all reactions. To simplify the physical module, dominant reactions are considered in the particle transport modeling. Atoms, hydrogen molecules, ions and electrons are the basic particles in fueling process. The plasma density, heat, and momentum transport equations together with neutral density and momentum transport equations are included in a seven-field fluid model that is deduced from the Braginskii equations [16] with some source and sink terms. In the equations, some basic transport physical effects are considered during the fueling process, including perpendicular plasma density diffusion, heat diffusion, parallel plasma density convection and heat conduction, energy interchange between ion and electron, parallel ion viscosity, atom diffusion and molecule radial density convection. The transport equations are cited and re-written as follows [17]:

$$\frac{\partial N_i}{\partial t} + \nabla_{\parallel}\left(V_{\parallel i} N_i\right) - D_{\perp i}^{c} \nabla_{\perp}^{2} N_i = S_I^{p} - S_{rec}^{p}, \tag{1}$$

$$\frac{\partial T_i}{\partial t} + V_{\parallel i}\nabla_{\parallel} T_i + \frac{2}{3} T_i \nabla_{\parallel} V_{\parallel i} - \frac{2}{3N_i}\nabla_{\parallel}\left(\kappa_{\parallel i}^{c}\nabla_{\parallel} T_i\right) - \frac{2}{3}\chi_{\perp i}^{c}\nabla_{\perp}^{2} T_i = \left(\nu_{rec} - \nu_I\right) T_i + \frac{2m_e}{M_i}\frac{T_e - T_i}{\tau_e}, \tag{2}$$

$$\frac{\partial V_{\parallel i}}{\partial t} + V_{\parallel i}\nabla_{\parallel} V_{\parallel i} - \frac{4}{3N_i M_i}\nabla_{\parallel}\left(\eta_i^{0}\nabla_{\parallel} V_{\parallel i}\right) = -\frac{\nabla_{\parallel} P}{N_i M_i} - \left(\nu_{CX} + \nu_I\right) V_{\parallel i}, \tag{3}$$

$$\frac{\partial T_e}{\partial t} - \frac{2}{3N_i}\nabla_{\parallel}\left(\kappa_{\parallel e}^{c}\nabla_{\parallel} T_e\right) - \frac{2}{3}\chi_{\perp e}^{c}\nabla_{\perp}^{2} T_e = \nu_{rec} W_{rec} - \nu_I\left(T_e + \frac{2}{3}W_I\right) - \frac{2}{3}\nu_{diss}\left(W_{diss} + W_{bind}\right) - \frac{2m_e}{M_i}\frac{T_e - T_i}{\tau_e}, \tag{4}$$

$$\frac{\partial N_a}{\partial t} - \nabla_{\parallel}\left(D_{\parallel a}^{c}\nabla_{\parallel} N_a\right) - D_{\perp a}^{c}\nabla_{\perp}^{2} N_a = -S_I^{p} + S_{rec}^{p} + 2S_{diss}^{p}, \tag{5}$$

$$\frac{\partial N_m}{\partial t} + \nabla_x\left(V_{xm} N_m\right) = -S_{diss}^{p}, \tag{6}$$

$$\frac{\partial V_{xm}}{\partial t} + V_{xm}\nabla_x V_{xm} = -\frac{\nabla_x P_m}{N_m M_m}. \tag{7}$$

The equations (1) - (4) describe plasma density, heat and momentum transport. Equation (5) is the atom density transport that is based on atom diffusion caused by the strong charge exchange collision rate. The last two equations describe molecular density and momentum transports. Perpendicular and parallel atom diffusions together with Plasma quasi-neutral condition ($N_i = N_e$) are considered in simulations. In equation (6) and equation (7), ∇_x represents the radial component of the gradient. The molecular pressure is $P_m = kN_m T_m$ where the molecule temperature is T_m (i.e., the room temperature). More details of the physical model could be found in the reference [17].

2.2 Boundary conditions

Figure 1 describes the fueling from low field side in realistic divertor geometry of the HL-2A tokamak. The poloidal cross-section can be divided into several regions [18]: wall, private flux region, scrape-off-layer (SOL) region, plasma edge, and core region. The geometry used in the simulation has an X-point where $\theta = 0$ and the positive poloidal direction is in clockwise rotation. Divertor plates are located at the poloidal angles $\theta = 0$ and $\theta = 2\pi$. Similar with the real tokamak magnetic field, the field-aligned coordinate (x, y, z) [18, 19] corresponds to the general flux coordinate (ψ, θ, ξ). In this paper, the simulation domain is $\psi = 0.65 \sim 1.1$ in the radial direction.

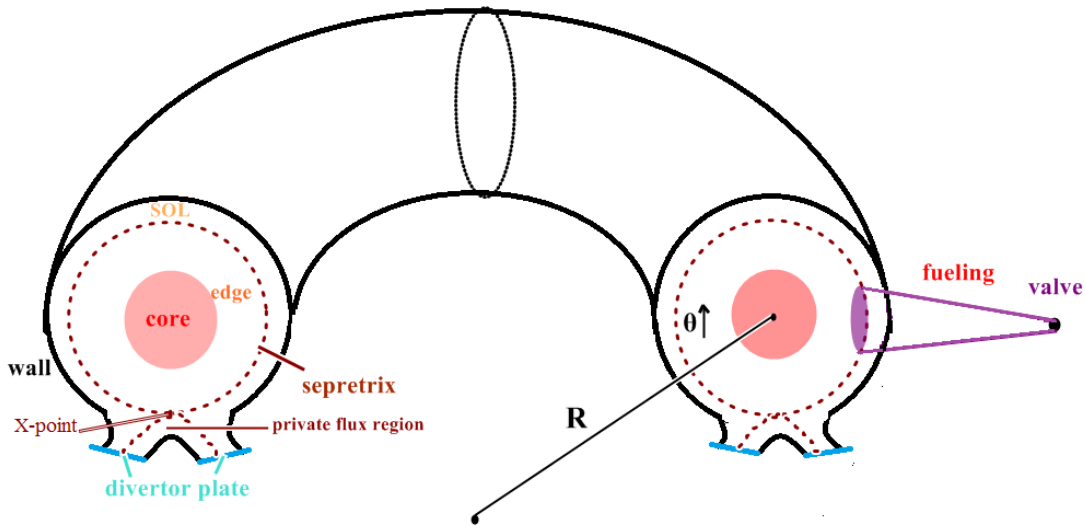

Figure1. A fueling configuration in HL-2A and different regions on tokamak poloidal cross-section

First, the radial*(x)* flux-driven boundary conditions are considered in simulations. They simulate the particle and heat fluxes that flow in from the innermost magnetic surface. The radial*(x)* flux-driven boundary conditions of N_i, T_i and T_e are set by fixed-gradients at core as follows:

$$\left.\frac{\partial N_i}{\partial x}\right|_{core} = -C_{Ni}\frac{N_0}{L_0^2 B_0}, \tag{8}$$

$$\left.\frac{\partial T_{e,i}}{\partial x}\right|_{core} = -C_{Te,i}\frac{T_0}{L_0^2 B_0}. \tag{9}$$

The normalization parameters are $T_0 = 10eV$, $N_0 = 10^{19}$, $L_0 = 5cm$ and $B_0 = 1.76T$, while the gradient coefficients are $C_{Ni} = 195$, $C_i = 25100$ and $C_e = 25100$. In private flux region, N_i, T_i and T_e are set by Dirichlet boundary conditions such as $N_i\big|_{pf} = 0.07N_0$ and $T_i\big|_{pf} = T_e\big|_{pf} = T_0$. At the outermost flux surface, T_i and T_e use Dirichlet boundary conditions, while N_i and N_a are set by particle recycling boundary conditions. The innermost and outermost boundaries of other variables are Neumann boundary conditions.

Second, GP and SMBI can be modeled by applying constant flux boundary conditions locally at edge, which is more realistic than simply giving a source term in the equations. The major difference between GP and SMBI is the initial injection velocity V_{xm0} in simulations. Fueling sources are injected with constant molecule fluxes localized in the poloidal *(y)* direction. The local constant flux boundary conditions with molecular density and injection velocity are as follows:

$$N_m\big|_{edge} = N_{m0}\exp\left(-\left(\theta-\theta_{1/2}\right)^2/\left(w_\theta/a\right)^2\right), \qquad \left(\theta_0 \le \theta \le \theta_1\right) \tag{10}$$

$$V_{xm}\big|_{edge} = V_{xm0}\exp\left(-\left(\theta-\theta_{1/2}\right)^2/\left(w_\theta/a\right)^2\right), \qquad \left(\theta_0 \le \theta \le \theta_1\right) \tag{11}$$

In the equations above, $\theta_{1/2} = \left(\theta_0+\theta_1\right)/2$ is the fueling source center and w_θ is poloidal width of fueling at the outermost boundary flux surface. In simulations, the parameters are $\theta_0 = 1.1\pi$, $\theta_1 = 1.3\pi$, $w_\theta = 12.5cm$, and $a = 40cm$, which are the same for both GP and

SMBI.

Third, as an electrostatic sheath is formed on the divertor plate, it can reflect all but high energy electrons so that the fluxes of ion and electron flowing into divertor plate will be the same. Sheath boundary conditions are as following:

$$V_{\square i}\Big|_{\theta=0} = -c_{se}\Big|_{\theta=0} \quad ; \quad V_{\square i}\Big|_{\theta=2\pi} = c_{se}\Big|_{\theta=2\pi}, \tag{14}$$

$$\nabla_{\square} N_i\Big|_{\theta=0} = 0 \quad ; \quad \nabla_{\square} N_i\Big|_{\theta=2\pi} = 0, \tag{15}$$

$$\nabla_{\square} T_{e,i}\Big|_{\theta=0} = \mathrm{Q}^{d}_{e,i} / \left(k\kappa^{c}_{\square e,i}\right)\Big|_{\theta=0} \quad ; \quad \nabla_{\square} T_{e,i}\Big|_{\theta=2\pi} = -\mathrm{Q}^{d}_{e,i} / \left(k\kappa^{c}_{\square e,i}\right)\Big|_{\theta=2\pi}. \tag{16}$$

In the equation (16), $\mathrm{Q}^{d}_{e,i} \equiv \gamma_{e,i} k T_{e,i} \Gamma^{d}_{i}$ presents the total transmission heat. The positive and negative values at $\theta = 0$ or 2π are relevant to the directions of local outgoing particle and heat fluxes.

At last, neutral particles attached on the wall and divertor plates can recycle back into plasma. Particle recycling boundary conditions [17] have also been included in the simulations.

3. Simulation results

The transport dynamics of GP and SMBI are studied with the same initial plasma conditions ($t = 0ms$). In the simulations, the durations of injecting pulses are $1ms$, a typical injection time of GP and SMBI. For GP, the injecting molecular density $N_m = 2\times10^{18}$, the injecting velocity $V_{m0} = 5m/s$, and the injecting width is $25cm$. For SMBI, the injecting molecular density and the injecting width are the same as GP, except the velocity $V_{m0} = 1000m/s$. The radial and poloidal transport dynamics during GP and SMBI will be compared as follows.

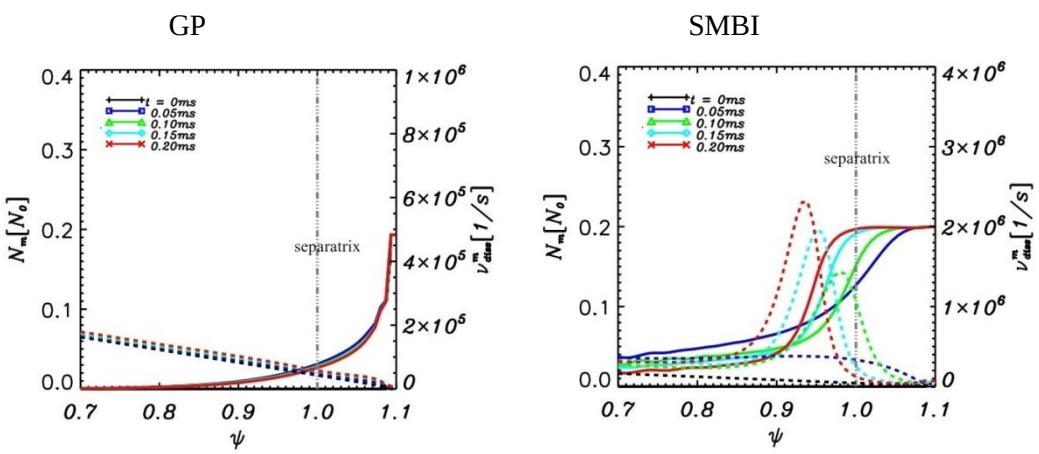

Figure 2. The time evolution of the molecular density $\mathrm{N_m}$ (solid curve) and the molecular

dissociation rate (dashed curve) within $0.2ms$, along the injection channel of molecules

First, the transport dynamics during GP and SMBI is compared in radial direction. There are no molecules at $t = 0ms$. In figure 2 (right), the molecular propagation front of SMBI can penetrate into the separatrix due to larger injection velocity. As the interval time between different solid curves is the same and the radial distance between solid curves is decreasing in figure 2 (right), the propagation speed of molecules is reduced with the increasing penetration depth. This is because the increasing molecule dissociation rate restrains molecule penetration. With the smaller injection velocity, molecules injected by GP (figure 2 (left)) are distributed in SOL region where its dissociation rate is very small.

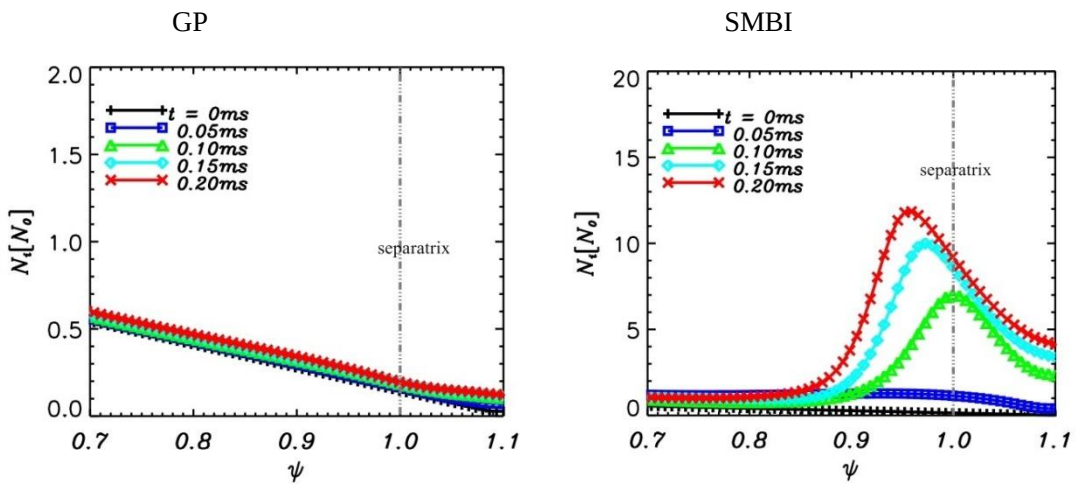

Figure 3. The time evolution of radial profile for ion density within $0.2ms$

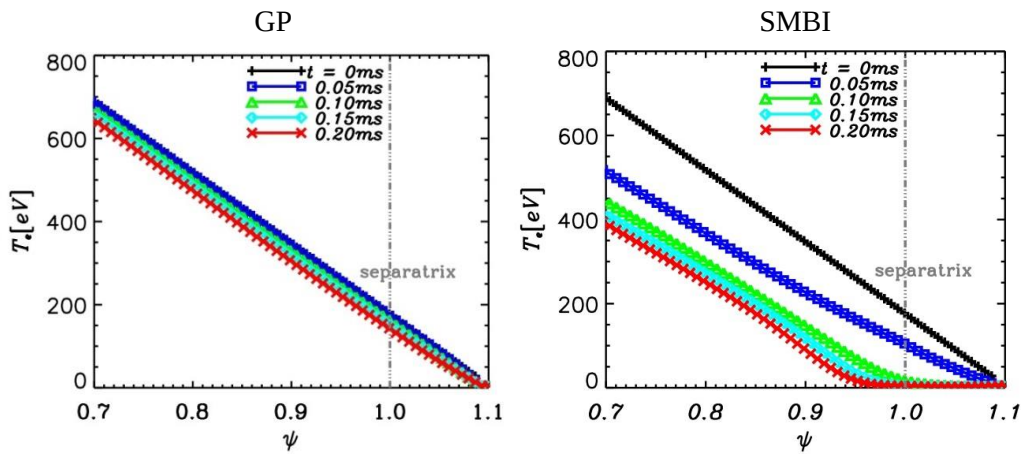

Figure 4. The time evolution of radial profile for electron temperature within $0.2ms$

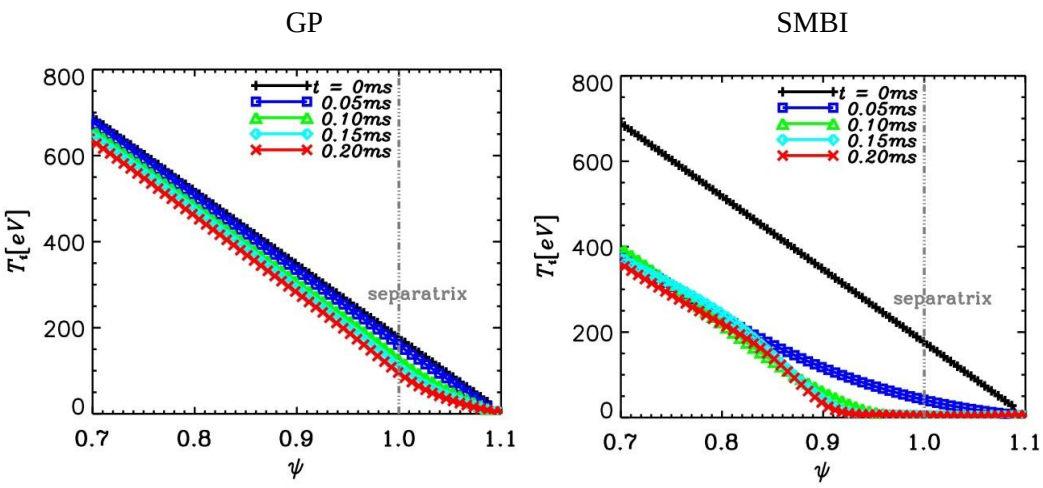

Figure 5. The time evolution of radial profile for ion temperature within $0.2ms$

With the inward neutrals propagation, N_i is locally increased along fueling path as figure 3. It's obvious that N_i grows slowly in the SOL region during GP (figure 3 (left)). N_i of SMBI (figure 3 (right)) increases dramatically near beam front where is around $\psi = 0.9$ (about 4cm deep inside the separatrix). It reveals that SMBI with higher injection velocity is more efficient to increase ion density inside the separatrix than GP. Along the fueling path, plasma temperature decreases during GP and SMBI in figure 4 and figure 5. This is because electrons lose energy during molecular dissociation, atom ionization and heat conductivity, while the ions lose energy during ion-electron energy exchange, dissociation, ionization, heat diffusion and heat conductivity. These cooling processes will be intensified by the increasing of plasma density during fueling. As ion density increasing more during SMBI, the plasma temperature is reduced more dramatically during SMBI than GP along radial direction. It reveals that SMBI is more efficient to cool the edge area with its higher injection velocity.

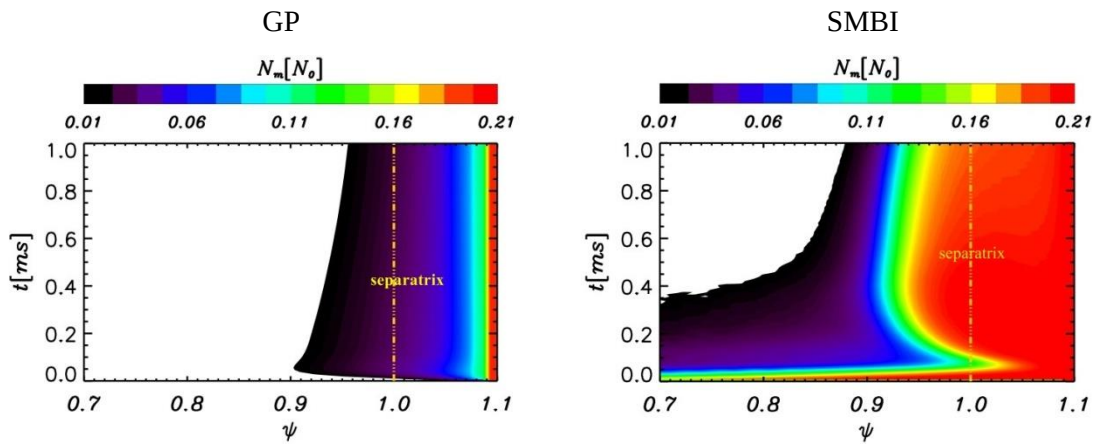

Figure 6. The time and spatial evolutions of molecular density for GP (left) and SMBI (right)

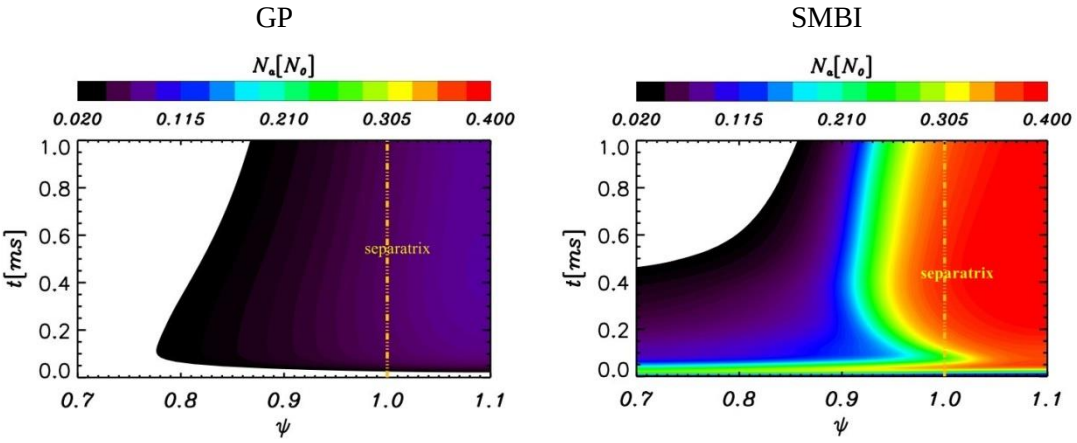

Figure 7. The time and spatial evolutions of atom density for GP (left) and SMBI (right)

Figure 6 indicates the most important information about the molecular injecting depth. The transport process of molecules during SMBI depends on radial convection due to its radial injection speed is much larger than its local thermal velocity. The molecules (figure 6 (right)) can be injected about $4cm$ deep inside the separatrix during SMBI. Besides, the molecular propagation front will move inward at beginning as the total molecular dissociation rate is not large enough. With the plasma density increasing at the propagation front, the molecular dissociation rate $R_m^{diss} = \int N_m \nu_{diss}^m dV$ (where ν_{diss}^m is proportional to plasma density) will become greater than the overall injection molecular rate $R_m^{in} = (N_m V_{xm} S_m)\big|_{edge}$. Then, the molecule propagation front retreats over time and will keep moving outwards after injection. Because it has a much slower injection speed and mainly depends on thermal diffusion during GP, the propagation front of molecules (figure 6 (left)) are deposited in SOL region. Based on the dissociation of molecules, N_a of GP (figure 7 (left)) is small and also mainly distributed in the SOL, while it can reach about $\psi = 0.9$ during SMBI (figure 7 (right)). Similar with N_m, the evolution of atom propagation front during SMBI depends on the competition between total atom ionization rate and total molecule dissociation rate.

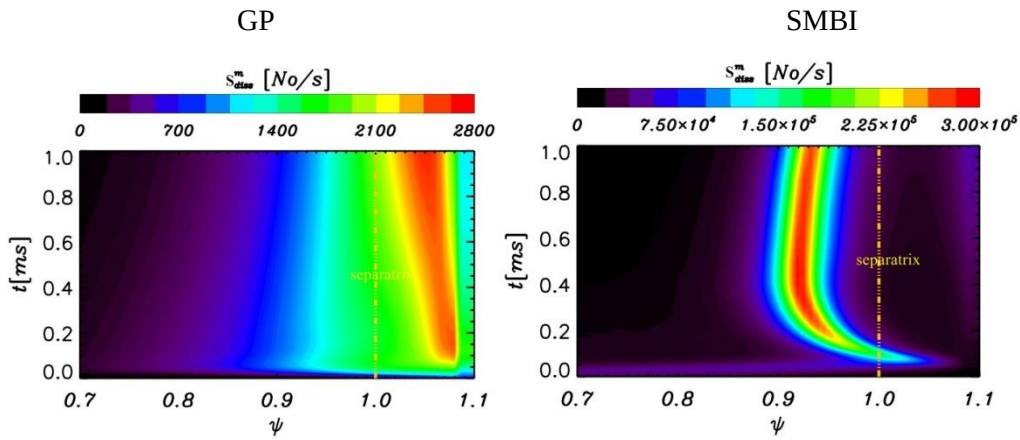

Figure 8. The time and spatial evolutions of molecular dissociation during GP (left) and SMBI

(right)

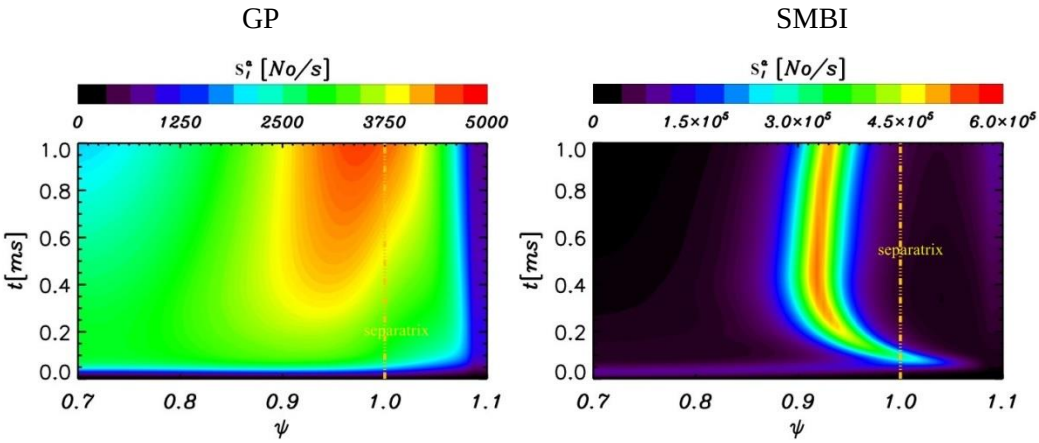

Figure 9. The time and spatial evolution of ionization during GP (left) and SMBI (right)

The dissociation source is $S_{diss}^{m} = v_{diss}^{m} \times Nm$. Most molecules injected by SMBI (figure 8 (right)) are dissociated around molecule propagation front where is inside the separatrix, due to the high radial injection velocity and great injection molecular flux. With a very small injection speed, molecules of GP mainly depend on thermal diffusion process so that the source of dissociation (figure 8 (left)) is situated in the SOL during GP. What is more, the scale of the molecular dissociation source during SMBI is about 2 orders greater than GP. In figure 9, the ionization source is $S_{\mathrm{I}}^{\mathrm{a}} = v_{I}^{m} \times Nn$ that decides the increase of ion density directly. Fewer atoms (figure 9 (left)) can penetrate into separatrix and be ionized during GP than SMBI, as it depends on molecular dissociation (i.e. one molecule be dissociated into two atoms). In figure 9 (right), it is clear that ionization region during SMBI is much deeper than GP. The regions of dissociation and ionization are just in a small area with SMBI. As a result, most neutrals injected by SMBI could be transformed into plasma inside the separatrix. It means that SMBI has higher fueling efficiency and deeper injection than GP.

From a different perspective, the following discussions about the injection transport properties are in poloidal direction.

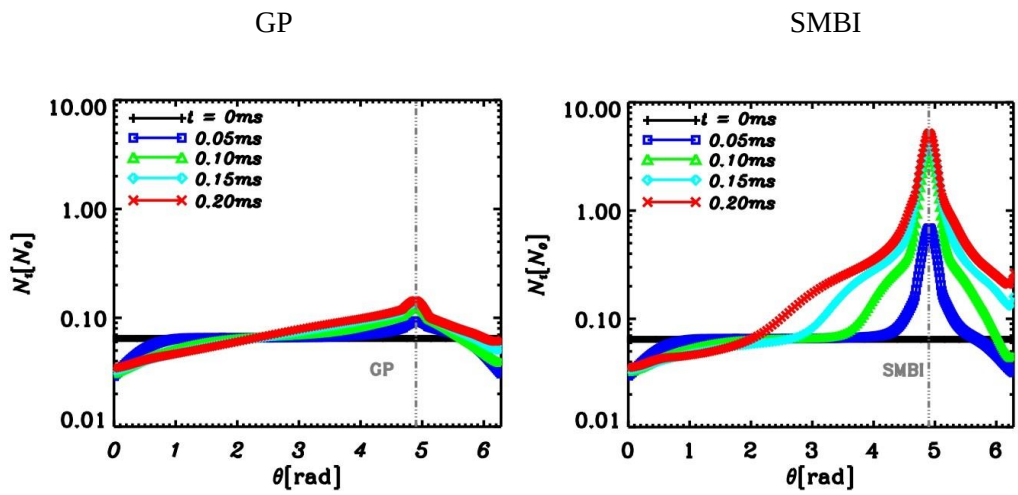

Figure 10. The time evolution of ion density on poloidal profile, plotted at $\psi = 0.98$ during GP and SMBI

In figure 10, the plasma density has a constant value in parallel direction at initial state. Plasma density in fueling region grows first during both GP and SMBI. Then, the nearby ion density also increases in poloidal direction, due to the parallel convection. With the greater injection velocity, SMBI can inject neutrals to $\psi = 0.9$. But, most neutrals of GP cannot penetrate into separatrix owing to its slower injection velocity. The different injection depth leads to the plasma density inside the separatrix growing intensively during SMBI and changing little during GP.

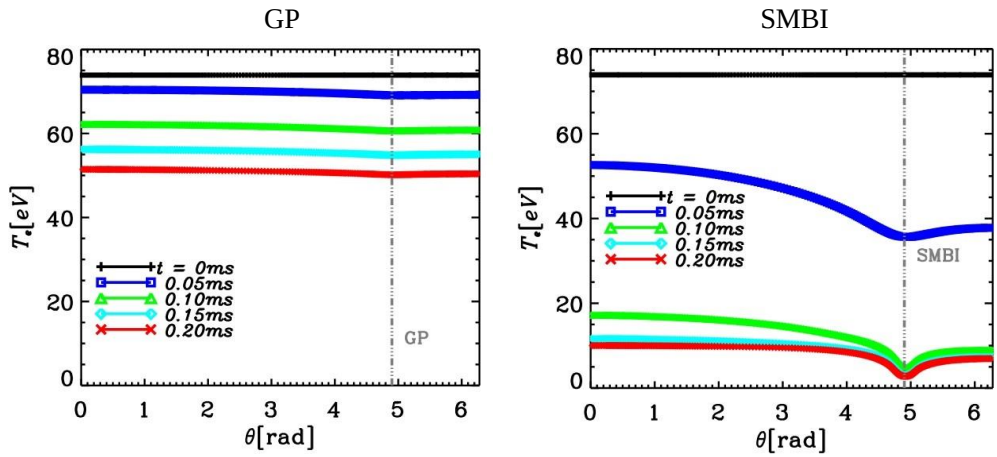

Figure 11. The time evolution of electron temperature on poloidal profile, plotted at normalized $\psi = 0.98$ during GP and SMBI

As figure 11 shows, the poloidal profiles of electron temperature are uniform in parallel direction that is plotted at $\psi = 0.98$ before fueling. Later with fueling, electron temperature is reduced in the fueling region first. Then, because of the parallel heat conductivity, the electron temperature around the fueling channel decreases over time. Owing to the higher molecule injection rate and deeper injection, the poloidal profiles of temperature plotted inside the separatrix (figure 11 (right)) vary larger during SMBI than GP (figure 11 (left)).

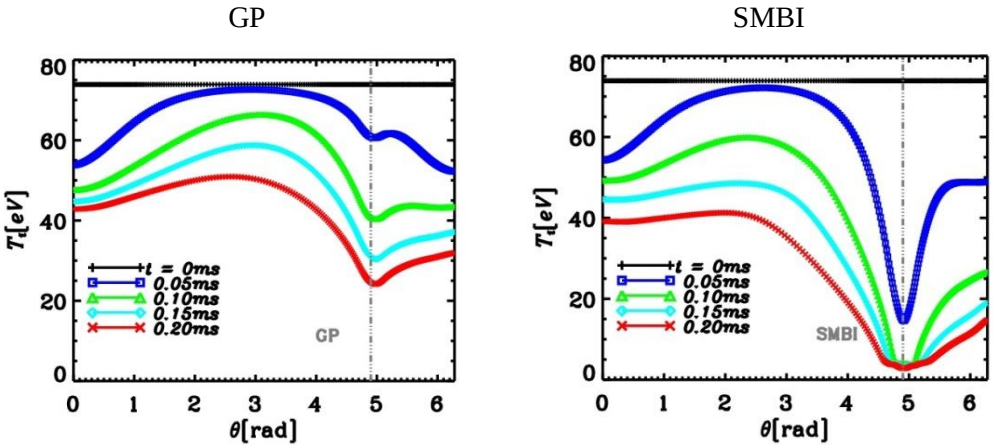

Figure 12. The time evolution of ion temperature on poloidal profile, plotted at normalized $\psi = 0.98$ during GP and SMBI

In figure 12, T_i is also reduced in poloidal direction during both GP and SMBI. Being different from electron thermal transport based on heat conductivity, ion thermal transport mainly depends on both heat conductivity and heat diffusion during fueling. The gradient of T_i around fueling path is larger than T_e due to the effect of parallel heat diffusion which is related to ion density distribution. Since N_i of SMBI (figure 10) increases more dramatically than GP in poloidal direction at $\psi = 0.98$, the gradient of T_i around injection beam (figure 12 (right)) is also larger during SMBI than GP.

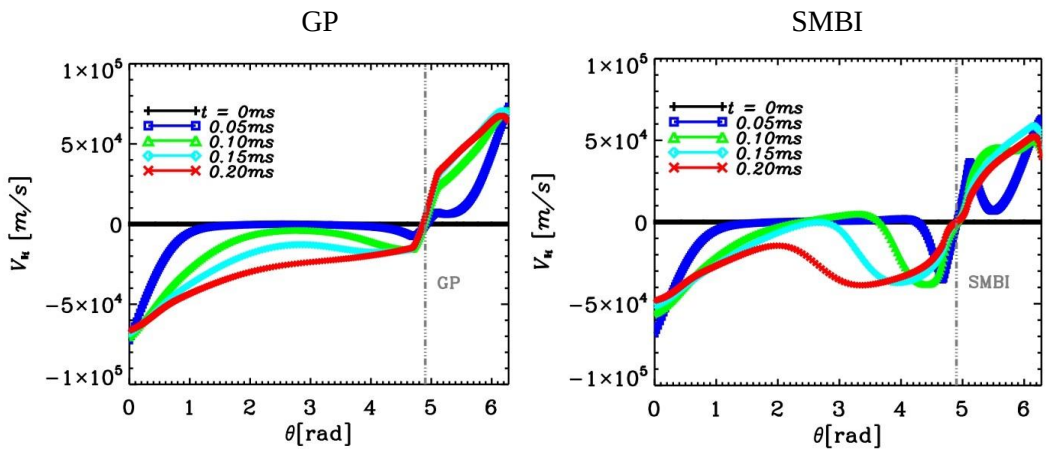

Figure 13. The time evolution of ion parallel velocity on poloidal profile, plotted at normalized $\psi = 0.98$ during GP and SMBI

In simulation, the places $\theta = 0$ and $\theta = 2\pi$ are coherent on plasma poloidal profile. At normalized $\psi = 0.98$ during fueling, the parallel ion speed is driven by the parallel pressure gradient which is related to ion density and temperature. As the gradients of ion density and

temperature at where SMBI injected is sharper than those of GP .It means that a larger parallel ion velocity can be driven during SMBI.

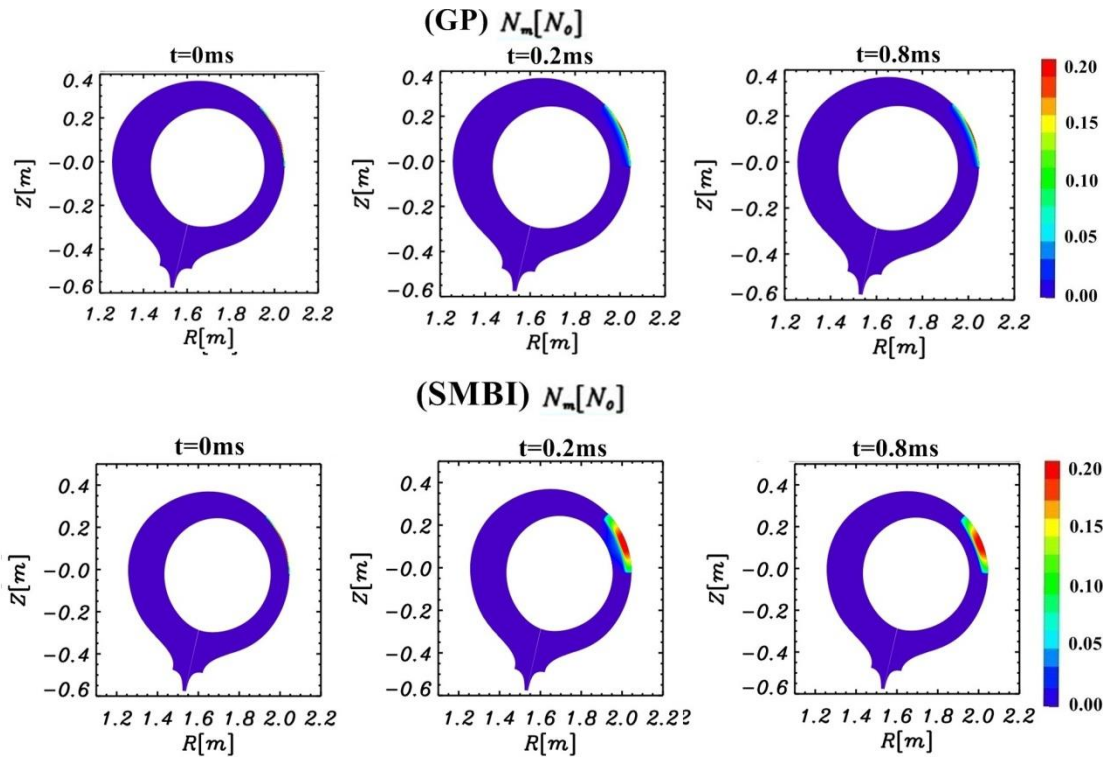

Figure 14. The poloidal evolution of molecular distribution plotted in cross-section of tokamak during SMBI and GP at different times

In figure 14, the poloidal distribution of molecular density is uniform before fueling. But after fueling from around $\theta = 1.2\pi$, the molecular density increases regionally. With a higher injection speed, the injection region of molecules during SMBI is much deeper than that of GP over time.

4. Summary

It is crucial to study neutral transport dynamics and find methods of improving the fueling performances such as high efficiency and deep injection. Two basic fueling methods, GP and SMBI, have been simulated and compared in realistic divertor geometry of the HL-2A tokamak with a newly developed module, named *trans-neut*, within the framework of BOUT++ boundary plasma turbulence code. Transport dynamics and profile evolutions of both plasma and neutrals are simulated and compared between GP and SMBI in both poloidal and radial directions, which are quite different from one and the other. The principal results are summarized as follows:

(1) Penetration depth of SMBI is deeper than GP mainly due to its much larger radial injection speed. Plasma initial states are the same before GP and SMBI. The boundary

conditions for GP and SMBI are the same except that SMBI has a much larger radial injection speed and a larger injecting molecular flux than GP. Molecules injected during SMBI can penetrate about 4cm inside the separatrix while the ones injected during GP are always deposited in the SOL region, which are consistent with the experiments. The penetrating speed of molecule front decreases with the increase of its penetration depth due to the increase of local molecule dissociation rate. When the molecule injection rate is larger than the overall molecular dissociation rate, the propagating front of molecules will keep penetrating deeper (i.e., SMBI). Since it has a much lower injection rate and it mainly depends on thermal diffusion process during GP, the propagating front of molecules can be saturated in SOL region even before it penetrates into the separatrix. It reveals that the key factor between GP and SMBI is the radial directed convection effect leading to the improvement of penetration depth.

(2) The ion density of SMBI grows more dramatically and in a much deeper region than GP owing to its deeper injection. The molecules dissociation and atoms ionization regions of SMBI are distributed at the propagation front of neutrals which is about 4cm inside the separatrix. On the other hand, the molecules dissociation area of GP is deposited in SOL region so that few neutrals are ionized inside the separatrix. In addition, the ion density during SMBI is about 2 orders more than GP. Thus, SMBI with greater injection velocity has a much higher efficiency to fuel inside the last closed (magnetic) flux surface (LCFS) than GP.

(3) Plasma profiles vary larger during SMBI than GP in both radial and poloidal directions. Since, SMBI has a much larger molecule injection rate than GP, plasma density increases and temperature profiles decrease dramatically in both radial and poloidal directions during SMBI, while the profiles change less during GP. Due to much shallow injection depth of GP, it is very hard for GP to change the plasma profiles along its injection channel especially inside the separatrix for a short injection time (i.e., 1ms) compared to SMBI. The pressure gradient at where SMB injected is sharper than that of GP which drives larger parallel ion velocity.

Neutral transport dynamics and profile evolutions during GP and SMBI have been simulated and compared. It reveals that SMBI with a much higher radial injection speed can effectively enhance the fueling depth and efficiency compared to GP. It thus suggests several further studies of this work on improving the fueling methods, as follows: 1) to study the transport dynamics during GP and SMBI with the same injection molecule flux ($\Gamma = S \times V \times N$) by varying the injection cross-section, speed and density. 2) to increase the injection time of GP and make sure the total molecule amount injected by GP equal to the one injected by SMBI, and study mean profile evolution. Even though plasma profiles will vary much more with more fueling particles injected, the penetration depth of GP will still not change since its injection rate does not change. The fueling efficiency of GP is lower than SMBI. Because its penetration depth is lower and most of the neutrals are pump out. Therefore, the fueling efficiency directly depends on the penetration depth. It is very interesting to find ways of

improving neutral penetration depth and efficiency and also give some hints for the experimentalists to improve the SMBI fueling method.

Acknowledgements

The authors wish to thank B. D. Dudson and M.V. Umansky for their contributions to BOUT++ framework. We also thank Y. Zhang, L. H. Yao, B. B. Feng, C. Y. Chen, and S. Y. Chen for their fruitful physical discussions. This work was supported by NSFC, Grant Nos. 11205053 and China National Magnetic Confinement Fusion Science Program, Grant 2013GB107001.

Prepared by LLNL under Contract DE-AC52-07NA27344.

References

[1] S. Sajjad, X. Gao, B. Ling, S. H. Bhatti and T. Ang, Phys. Lett. A, 2009. **373**: p. 1133-1139.

[2] L. R. Baylor, T. C. Jernigan, S. K. Combs, et al., Phys. Plasmas, 2000. **7**: p. 1878.

[3] L. H. Yao, D. W. Zhao, B. B. Feng et al., Plasma Sci. and Technol., 2010. **12**: p. 529

[4] W. Treutterer, G. Neu, G. Raupp, D. Zasche et all., Fusion Engineering and Design 81(2006) 1927-1931

[5] W. Treutterer, plasma shape control design in ASDEX Upgrade, Proceedings 19th SOFT, Lisbon, 1996,pp. 933-936.

[6] Tobita K, et al., Nucl Fusion 49(2009) 075029

[7] Kwon M, et al., 'Overview of KSTAR Initial Operation' Fusion Energy Conference 2010 (Proc. 23th Int. Conf. Daejeon), OV1-1

[8] D.L. YU, C.Y. Chen, L.H. Yao et al., Nucl. Fusion, 2012.07:p. 52

[9] W. W. Xiao, P. H. Diamond, W. C. Kim et al., Nucl. Fusion, 2014.54: p.023003.

[10] B. J. Braams, *Computational studies in tokamak equilibrium and transport*. 1986, State University: Utrecht, Netherlands.

[11] T. D. Rognlien, B. J. Braams, and D. A. Knoll, Contrib. Plasma Phys., 1996. **36**: p. 105.

[12] T. D. Rognlien, D. D. Ryutov, N. Mattor, and G. D. Porter, Phys. Plasmas, 1999. **6**: p. 1851.

[13]I. Landman and G. J. Janeschitz, Nucl. Mater., 2007. **363-365**: p. 1061.

[14] W. W. Xiao, P. H. Diamond, X. L. Zou et al., Nucl. Fusion, 2012. **52**: p. 114027.

[15] B. D. Dudson, M. V. Umansky, X. Q. Xu, P. B. Snyder, and H. R. Wilson, Computer Physics Communications, 2009. **180**: p. 1467-1480.

[16] S. I. Braginskii, ed. *Reviews of Plasma Physics*. ed. M.A. Leontovich. Vol. 1. 1965, Consultants Bureau: New York. 205.

[17] Z. H. Wang, X. Q. Xu, T. Y. Xia and T. D. Rognlien., Nucl. Fusion 54(2014) 043019 (16pp)

[18] X. Q. Xu, M. V. Umansky, B. Dudson, and P. B. Snyder, Commun. Comput. Phys., 2008. **4**: p. 949-979.

[19] M. V. Umansky, X. Q. Xu, B. Dudson, L. L. LoDestro, and J. R. Myra , Computer Physics Communications, 2009. **180**: p. 887-903.